CubeSat Autonomous Orbit Determination Based on Magnetometer and Sun Sensor Data

Wesam Mohammed Elmahy, *Zhang Xiang* *, *Lu Zhengliang*, *Liao Wenhe*

School of Mechanical Engineering, Nanjing University of Science and Technology, Nanjing 210094, P. R. China

(Received 18 June 2017; revised 20 November 2017; accepted 20 November 2017)

Abstract: CubeSats have evolved from purely educational tools to a standard platform for technology demonstration, scientific instrumentation and application in less than a decade. They open the door to new challenges and interplanetary missions which lead to the direct realization of autonomous orbit determination (AOD) which has been investigated before with different integrated sensors combined with various filters. Mostly these studies were carried out for larger satellites with more accurate sensors. Magnetometer and sun sensor combined with extended Kalman filter (EKF) are chosen to complete AOD task considering their light weight. For the purpose of AOD and the computational cost requirements imposed on CubeSats, it is important to develop and apply low cost on-board models. In this perspective, a magnetic model based on a table look up is proposed to generate the reference magnetic field with a low computational burden. In current article the simulations through Matlab and Satellites Tool Kit (STK) especially focus on the accuracy of the AOD system provided by this model. For analysis three EKFs are carried out with different calculation models and data types. The system based on the proposed model is fully autonomous, low-cost and has moderate-accuracy required by most CubeSats missions. The AOD system can be applied as main or backup system depending on the space missions' demands.

Key words: CubeSat; autonomous orbit determination (AOD); magnetometer; sun sensor

CLC number: V412.4 **Document code**: A **Article ID**: 1005-1120(2017)06-0700-10

0 Introduction

In recent years a significant increase in interest with smaller satellites has appeared. These satellites are commonly used for educational purposes or as technology demonstrators[1]. CubeSats were originally proposed as means of reducing satellite costs to enable academic participation in space science[2-3]. Accturally, CubeSats are a subcategory of nanosatellites, but the names are used interchangeably a lot in manuscripts. CubeSats have gathered international attention and approximately several hundreds have been launched by universities, research institutes, and commercial entities with demonstrating active attitude, determination, control systems (ADCS). In addition, they also interned many applications as formation flying[4]. Due to strict mass, size, and budget constraints placed on these satellites, they typically rely on simple sensor hardware. Emphasis is placed on balancing accuracy with computational costs to improve autonomy, reduce ground testing and support costs.

A variety of autonomous orbit determination (AOD) methods have been proposed and explored, using different types of sensors. Magnetometer-based and celestial orbit determination (OD) methods are particularly suitable to be used in low earth orbits (LEO)[5]. Magnetometer was first introduced by Psiaki for AOD[6]. The idea of using magnetometer in OD was to compare the onboard measurements with a spherical harmonic model and use it to correct the state of the satellite. He used a batch filter and it took a long time

* Corresponding author, E-mail address: zhxiang2002@126.com.

How to cite this article: Wesam Mohammed Elmahy, Zhang Xiang, Lu Zhengliang, et al. CubeSat autonomous orbit determination based on magnetometer and sun sensor[J]. Trans. Nanjing Univ. Aeronaut. Astronaut., 2017,34(6):700-709. http://dx.doi.org/10.16356/j.1005—1120.2017.06.700

to converge. A batch filter is also unsuitable for real-time data applications. Psiaki's work was attitude independent, as well as, Wiegand[7]. Wiegand used a magnetometer and EKF based OD method and examined using real flight data of the BREM-SAT mission. He expected that less than 10 km position error can be achieved if a precise magnetometer was used and recommended the system for small satellites. The magnetometer measurements were also combined with a particle filter (PF)[8] and with unscented Kalman filter (UKF)[9] in attempt to try various filters in OD providing better accuracy. Successful attempts have also been made to use magnetometer measurements to find both the attitude and the orbit of satellites[10-11]. Shorshi and Bar-Itzhack achieved accuracy on the order of 10—35 km when tested with real flight data[12].

Magnetometers are the least accurate compared to other sensors. Different sensors are combined with magnetometer for better accuracy and performance. The integration of the magnetometer and other sensors was previously investigated. Psiaki integrated the magnetometer with Sun sensor data arriving at 300 m position error[13]. He also combined magnetometer and star sensor data and reached 500 m position error[14]. The horizon sensor was combined with magnetometer along with the UKF[15]. A less than 500 m accuracy of position and 1 m/s accuracy in velocity were found with 0.1 nT magnetometer and 0.051° horizon sensor. Clearly this work was performed by more accurate sensors that cannot be found on-board CubeSats. Celestial and geomagnetic measurements were also applied with different filters[16]. The previous studies were performed for large satellites and most of them indicated the suitability of the proposed systems for AOD in smaller satellites. Few studies applied the AOD in Picosats and CubeSats[17]. These studies integrated magnetometer, Sun sensor and EKF for OD, as they are the lightest in all sensors.

In the study by Rikard[18] the absolute position error was found to be 19.08 km using only magnetometer data. But using magnetometer and Sun sensor data, the average RSS was 14.90 km, recording improvement in the settling time. He applied the international geomagnetic reference field (IGRF) model in his work to generate the state estimates. His algorithm was also tested using real flight data, and the filter converged to an average RSS error of 56.52 km within twelve hours.

Few studies indicated the types of models that they applied in their work. Even if it was indicated that most of these models were neither suitable nor realistic to be used on-board CubeSats, it would be essential to apply low cost on-board models to the AOD task. This is an important aspect to be considered.

The same integrated system used in Ref.[19] is also applied here but with a different magnetic model in the estimation process. We propose a magnetic model based on a table look up which is adopted to generate the reference magnetic field. By this table, most of the computing resources can be saved. This is not only particularly reasonable for the power restrictions imposed on CubeSats but also needed when numerical integration is selected for propagation. The magnetic table presents a more realistic option for CubeSat applications rather than the IGRF model. The accuracy of the table applied in AOD here was not presented before in previous studies.

1 Autonomous Orbit Determination Method

Satellite orbit determination Method is based on predictor-corrector scheme which is used generally for real-time orbit determination. EKF is chosen for that purpose. A suitable state vector representation should also be selected and it depends on the solution procedure.

1.1 Predictor-corrector scheme (EKF)

The EKF is constructed by linearizing either the system equation or the measurement equation or both about the current (predicted) state estimate using the first two terms of a Taylor series

expansion and using structure of the linear Kalman filter to provide the next estimate[20]. EKF Equations, which are widely known are summarized here for clarity.

EKF prediction equations:

Predicted state estimate vector is given by

$$\hat{\boldsymbol{x}}_{k/k-1} = f(\hat{\boldsymbol{x}}_{k-1/k-1}, \boldsymbol{u}_{k-1}) \tag{1}$$

Its corresponding error covariance matrix is given by

$$\boldsymbol{P}_{k/k-1} = \boldsymbol{\Phi}_{k-1}\boldsymbol{P}_{k-1/k-1}\boldsymbol{\Phi}_{k-1}^{\mathrm{T}} + \boldsymbol{Q}_{k-1} \tag{2}$$

EKF update equations:

The innovation sequence or the measurement residual vector reflects the degree to which level the model fits the data, it is given by

$$\boldsymbol{\Psi}_k = \boldsymbol{z}_k - h(\hat{\boldsymbol{x}}_{k/k-1}) \tag{3}$$

The covariance matrix of innovation sequence is given by

$$\boldsymbol{S}_k = \boldsymbol{H}_k\boldsymbol{P}_{k/k-1}\boldsymbol{H}_k^{\mathrm{T}} + \boldsymbol{R}_k \tag{4}$$

Kalman Gain matrix

$$\boldsymbol{K}_k = \boldsymbol{P}_{k/k-1}\boldsymbol{H}_k^{\mathrm{T}}\boldsymbol{S}_k^{-1} \tag{5}$$

Update state estimate vector

$$\hat{\boldsymbol{x}}_{k/k} = \hat{\boldsymbol{x}}_{k/k-1} + \boldsymbol{K}_k\boldsymbol{\Psi}_k \tag{6}$$

Its corresponding error covariance matrix

$$\boldsymbol{P}_{k/k} = \boldsymbol{E}[(\boldsymbol{x}_k - \hat{\boldsymbol{x}}_{k/k})(\boldsymbol{x}_k - \hat{\boldsymbol{x}}_{k/k})^{\mathrm{T}}] = (\boldsymbol{I} - \boldsymbol{K}_k\boldsymbol{H}_k)\boldsymbol{P}_{k/k-1} \tag{7}$$

where $\boldsymbol{x}_k$ is the state vector, $f(\boldsymbol{x}_k, \boldsymbol{u}_k)$ is a suitable vector function which defines the state transition from $\boldsymbol{x}_k$ to $\boldsymbol{x}_{k+1}$ using the deterministic input $\boldsymbol{u}_k$ and the process random noise $\boldsymbol{w}_k$ occurring at time k, while $\boldsymbol{z}_k$ is the observation vector, $h(\boldsymbol{x}_k)$ the measurement function and $\boldsymbol{v}_k$ the vector that represents the measurement error sources. $f(\boldsymbol{x}_k, \boldsymbol{u}_k)$ and $h(\boldsymbol{x}_k)$ are in general nonlinear functions where linearization of these nonlinear functions is essential to obtain a real time implementable algorithm. The process noise $\boldsymbol{w}_k$ and the measurement noise $\boldsymbol{v}_k$ are zero mean, white Gaussian random sequences, respectively. The initial state $\boldsymbol{x}_0$ is a Gaussian random vector with zero mean and covariance $\boldsymbol{P}_0$. It is assumed that $\boldsymbol{w}_k$, $\boldsymbol{v}_k$, $\boldsymbol{x}_k$, and $\boldsymbol{x}_0$ are mutually independent.

To prevent the Kalman filter divergence, in this research, the following algebraically equivalent covariance correction equation, which is called "Joseph flternative KF form"[19], is applied

$$\boldsymbol{P}_{k/k} = (\boldsymbol{I} - \boldsymbol{K}_k\boldsymbol{H}_k)\boldsymbol{P}_{k/k-1}(\boldsymbol{I} - \boldsymbol{K}_k\boldsymbol{H}_k)^{\mathrm{T}} + \boldsymbol{K}_k\boldsymbol{R}_k\boldsymbol{K}_k^{\mathrm{T}} \tag{8}$$

where the symmetry of the matrix multiplication forces $\boldsymbol{P}_{k/k}$ to remain symmetric.

1.2 Dynamic model

For a continuous system, there are different forms for the state vector representation. Each form depends on the solution procedure and the analysis type. In this work, the position and velocity vectors, in the earth centered inertial (ECI) coordinates frame, are used to represent the state. This form is more suitable for numerical processing and usually easier to deal with during the OD process since they have no singularities. The state is presented as follows

$$\boldsymbol{x}(t) = \begin{bmatrix}\boldsymbol{r}\\ \boldsymbol{v}\end{bmatrix}_{\mathrm{ECI}} \quad \boldsymbol{r} = \begin{bmatrix}x\\ y\\ z\end{bmatrix} \quad \boldsymbol{v} = \begin{bmatrix}\dot{x}\\ \dot{y}\\ \dot{z}\end{bmatrix} \tag{9}$$

The dynamic model of the state describes how it changes relative to time. The state propagation can be written as

$$\dot{\boldsymbol{x}}(t) = f(\boldsymbol{x}(t)) + \boldsymbol{w}(t) = \begin{bmatrix}\boldsymbol{v}(t)\\ \boldsymbol{a}(t)\end{bmatrix} + \boldsymbol{w}(t) = \begin{bmatrix}\dot{x}\\ \dot{y}\\ \dot{z}\\ a_x\\ a_y\\ a_z\end{bmatrix} + \begin{bmatrix}0\\ 0\\ 0\\ w_1\\ w_2\\ w_3\end{bmatrix} \tag{10}$$

The order of the total acceleration used in current work is equal to Newton's acceleration and the acceleration perturbation due to J2 (second zonal harmonic effect) is suitable for orbits in altitudes higher than 600 km.

Therefore, the acceleration components a_x, a_y and a_z are represented in the ECI frame, as

$$\begin{aligned}
a_x &= a_{x_{\mathrm{Newton}}} + a_{x_{J2}} = -\frac{\mu x}{r^3} + \frac{\mu J_2 R^2}{2}\left(15\frac{xz^2}{r^7} - 3\frac{x}{r^5}\right)\\
a_y &= a_{y_{\mathrm{Newton}}} + a_{y_{J2}} = -\frac{\mu y}{r^3} + \frac{\mu J_2 R^2}{2}\left(15\frac{yz^2}{r^7} - 3\frac{y}{r^5}\right)\\
a_z &= a_{z_{\mathrm{Newton}}} + a_{z_{J2}} = -\frac{\mu z}{r^3} + \frac{\mu J_2 R^2}{2}\left(15\frac{z^3}{r^7} - 9\frac{z}{r^5}\right)
\end{aligned} \tag{11}$$

where r is the norm of the vector between the center of the Earth and the satellite, the standard gravitational parameter $\mu = 3.986\,004\,418 \times 10^{14}\ \mathrm{m^3 s^{-2}}$

defined as the product of the universal constant of gravitation $G=6.673\ 84\times10^{-11}\ \mathrm{m^3/(kg\cdot s^2)}$ and the mass of the Earth $m_{\mathrm{Earth}}=5.972\times10^{24}\ \mathrm{kg}$, the dimensional coefficient $J_2=0.00\ 108\ 27$ has been found from satellite observations and the radius of the Earth $R=6\ 378.137\ \mathrm{km}$ at the equator.

1.3 Propagation step

As the state is propagated forward in time, the confidence of the state will degrade over time due to the force model errors. These errors arise from the unmodeled acceleration. The change in the covariance can be written as[18-19]

$$\dot{\boldsymbol{P}}=\boldsymbol{\Phi P}+\boldsymbol{P\Phi}^{\mathrm{T}}+\boldsymbol{Q} \tag{12}$$

To calculate the covariance matrix $\boldsymbol{P}$, the first Jacobian matrix ($\boldsymbol{\Phi}$) is needed, and it is given by

$$\boldsymbol{\Phi}=\left.\frac{\partial f}{\partial x}\right|_{\hat{\boldsymbol{x}}_{\frac{k}{k}},\boldsymbol{u}_k}=\boldsymbol{\Phi}(\bar{\boldsymbol{x}}(t))=$$

$$\left[\begin{array}{cccccc}0&0&0&1&0&0\\0&0&0&0&1&0\\0&0&0&0&0&1\\\dfrac{\partial a_x}{\partial x}&\dfrac{\partial a_x}{\partial y}&\dfrac{\partial a_x}{\partial z}&0&0&0\\\dfrac{\partial a_y}{\partial x}&\dfrac{\partial a_y}{\partial y}&\dfrac{\partial a_y}{\partial z}&0&0&0\\\dfrac{\partial a_z}{\partial x}&\dfrac{\partial a_z}{\partial y}&\dfrac{\partial a_z}{\partial z}&0&0&0\end{array}\right]_{\boldsymbol{x}(t)=\bar{\boldsymbol{x}}(t)} \tag{13}$$

The numerical Runge-Kutta method of the fourth order is used to propagate the state and covariance in-between measurements. It provides good performance to a relatively low computational cost even for larger integration steps [21].

1.4 Measurement model

The sensors used by Kalman filter here are a 3-axis magnetometer and a 2-axis Sun sensor, as in Ref. [18]. The outputs can be described as

$$\boldsymbol{B}_{\mathrm{meas}}=\boldsymbol{A}_{\mathrm{att}}\boldsymbol{B}_{\mathrm{act}}+v_1,\ \boldsymbol{S}_{\mathrm{meas}}=\boldsymbol{A}_{\mathrm{att}}\boldsymbol{S}_{\mathrm{act}}+v_2 \tag{14}$$

where $\boldsymbol{B}_{\mathrm{meas}}$ and $\boldsymbol{S}_{\mathrm{meas}}$ are the instant sample data of magnetometer and Sun sensor, representing the measured magnetic field vector and the measured sun direction normalized in satellite's body axis, respectively, $\boldsymbol{B}_{\mathrm{act}}$ and $\boldsymbol{S}_{\mathrm{act}}$ the actual magnetic field and Sun vectors, respectively. Both of which are expressed in ECI frame of reference. $\boldsymbol{A}_{\mathrm{att}}$ is the rotation matrix of satellite attitude. It is seen from Eq. (14) that the knowledge of attitude is needed. v_1 and v_2 are the noise variables described by

$$E(v_1)=0,E(v_1v_1)=\sigma_m^2,E(v_2)=0$$
$$E(v_2v_2)=\sigma_{\mathrm{m}}^2+\boldsymbol{B}_{\mathrm{meas}}^{\mathrm{T}}(\boldsymbol{I}-\boldsymbol{S}_{\mathrm{meas}}\boldsymbol{S}_{\mathrm{meas}}^{\mathrm{T}})\boldsymbol{B}_{\mathrm{meas}}\sigma_s^2 \tag{15}$$

To perform pure orbit estimation, new measurements that are independent of satellite attitude but retain all of the position/orbit information, should be developed. The simulated measurements have been manipulated to yield pseudo "measurements". The first is the measured magnetic field strength, and the second one is the measured cosine of the angle between the earth's magnetic field and the direction towards the Sun[17].

The pseudomeasurements can be calculated as

$$z_1=\sqrt{\boldsymbol{B}_{\mathrm{meas}}^{\mathrm{T}}\boldsymbol{B}_{\mathrm{meas}}}\approx\sqrt{\boldsymbol{B}_{\mathrm{act}}^{\mathrm{T}}\boldsymbol{B}_{\mathrm{act}}}+v_1$$
$$z_2=\frac{\boldsymbol{B}_{\mathrm{meas}}^{\mathrm{T}}\boldsymbol{S}_{\mathrm{meas}}}{\sqrt{\boldsymbol{B}_{\mathrm{meas}}^{\mathrm{T}}\boldsymbol{B}_{\mathrm{meas}}}}\approx\frac{\boldsymbol{B}_{\mathrm{act}}^{\mathrm{T}}\boldsymbol{S}_{\mathrm{act}}}{\sqrt{\boldsymbol{B}_{\mathrm{act}}^{\mathrm{T}}\boldsymbol{B}_{\mathrm{act}}}}+v_2 \tag{16}$$

The measurement model can be rewritten as

$$\boldsymbol{z}_k=h(\boldsymbol{x}_k)+\boldsymbol{v}_k,\boldsymbol{z}_k=\begin{bmatrix}z_1\\z_2\end{bmatrix},\boldsymbol{v}_k=\begin{bmatrix}v_1\\v_2\end{bmatrix} \tag{17}$$

In the case of magnetometer-sun sensor based filters, the 2×6 observation Jacobian matrix is given by

$$\boldsymbol{H}_k=\left.\frac{\partial h_k(x(t_k))}{\partial x}\right|_{\hat{\boldsymbol{x}}_{\frac{k}{k}-1}}=\begin{bmatrix}H_{11_k}&H_{12_k}&H_{13_k}&0&0&0\\H_{21_k}&H_{22_k}&H_{23_k}&0&0&0\end{bmatrix} \tag{18}$$

In the magnetometer based filter, $\boldsymbol{H}_k$ will only be a 1×6 vector represented by the first row of $\boldsymbol{H}_k$.

For the dual filter the pseudo-measurements are calculated from the magnetic and the sun sensor models at the predicted state estimate, the models implemented in this study are in subsection 2.1.1. The measurements will only depend on the position part of the state and not the velocity. That is why the last three elements of each row of $\boldsymbol{H}_k$ are set to zeros. The three elements of each row of matrix $\boldsymbol{H}_k$ are calculated using finite differencing [18]. This means that the partial derivatives of the pseudo-measurements are calcu-

lated numerically by evaluating the models at three positions around the state estimate and calculating the difference between these values and the value at the state estimate, and then divided by the step size. For simplicity, the distances are set to be equals as $d_x = d_y = d_z = 1$ km.

The magnetometer based filter is computed in the same way. The state is then updated using the magnetometer and Sun sensor measurements, the predicted covariance matrix will be computed based on equations of subsection 1.1.

2 Simulation Scenario

2.1 Scenario definition

In this section, three different autonomous nanosatellite algorithms with different structures are tested together. The definition of applied EK filters are shown Table 1 . Filter 1 processes magnetometer data only while Filters 2 and 3 include magnetometer and Sun sensor data. The EKF requires to compare the measurements with their expected values. These expected values are obtained from models of the Earth′s magnetic field and Sun vector model. Two magnetic models are used, a magnetic model based on a table look up and IGRF. The formal is applied in Filters 1 and 2 and the latter is applied in Filter 3. The pure filter performance can be seen clearly through Filter 3, as the error in the reference models is not present.

Table 1 Filters′ scenarios

Filter No.	Data type for processing	Magnetic reference model
1	Magnetometer only	Magnetic table
2	Magnetometer + Sun sensor	Magnetic table
3	Magnetometer + Sun sensor	IGRF11

2.1.1 Reference models and simulated measurements

(1) Magnetic table

To every geographic position, the direction and magnitude of Earth′s magnetic field are almost constant in a short time span. Thus, a table of Earth′s magnetic field can be created by dividing a sphere into finite number of indexes. There exist 10 682 indexes in this setup. The step of longitude index is set as 3°, from 0° up to 357°, and the step of latitude index is set as 2°, from −88° up to 88°. Two more indexes are needed to store data from North/South Pole. By using this magnetic table, most of the computing resources for operating the filters are saved with of course less accuracy provided. The model can be applied for circular orbits only and it has to be modified for each altitude assigned for the satellite. Until now this restriction is not a problem as most Nanosats are launched in circular ones.

(2) IGRF

IGRF is a series of mathematical models describing the large-scale internal part of the Earth′s magnetic field between epochs 1900 A. D. and the present. IGRF has been maintained and produced by an international team of scientists[22]. IGRF11 is applied in the current work. The magnetic field rotates with the earth, so in order to calculate the field it will depend on the position above the ground. Thus the inputs of the magnetic model are in earth centered earth fixed (ECEF) frame and hence to find the reference magnetic field in the filters, the position part of the state vector is first converted from ECI to ECEF coordinates.

(3) Sun model

The Sun vector model is based on the theory described by Vallado[23]. The motion of the planet around the Sun is the only variable that the Sun vector model used in the filter. It provides coarse accuracy.

(4) Reference model

The reference state is generated from the high-precision orbit propagator (HPOP) in STK. In the configuration, the Runge-Kutta 7/8 method for the numerical integration of the equations of motion, the EGM 96 model (up to a degree of 21 * 21) for perturbation due to the nonsymmetrical geopotential, the Jacchia-Roberts model for atmospheric drag, lunar/solar gravitational attraction and solar radiation pressure are also included. The atmospheric drag coefficient is set to 2.2, the solar radiation pressure coefficient is set

to 1.0 and the constant area-to-mass ratio is set to 0.004 3. Corresponding better to real data, zero mean Gaussian noise is added to the initial state.

(5) Simulated measurements

The IGRF11 and the Sun vector model as described previously are both used to generate the simulated measurements. Zero mean Gaussian noise is added in order to enhance the correspondence to real measurements. Measurement noise with 2 mG (200 nT), standard deviation is added to each component of the magnetic field vector and 0.051 7 to each component of the sun Vector. The sampling time interval is 20. No eclipses are simulated.

2.1.2 Acceleration model accuracy

A test is applied to prove the suitability of the dynamic model described in subsection 1.2. For that reason it is compared with a dynamic model including J4 and drag effects. A simplified drag model is used with a static density model to keep calculations as minimum as possible. A sun synchronous orbit at 700 km is chosen as a test case.

The Jacobian will be computed as two bodies with J2 perturbations in both cases. Filter 3 is used in this test, also a small initial error in the state is preferred so that the effect of the propagation model can be seen . The filter initial state vector was set as

$$\boldsymbol{r}_o = \boldsymbol{r}_{\text{true}} + [30 \quad 30 \quad 30] \quad \text{km}$$
$$\boldsymbol{v}_o = \boldsymbol{v}_{\text{true}} + [10 \quad 10 \quad 10] \quad \text{m/s} \qquad (19)$$

And the initial covariance is set as

$$\boldsymbol{P}_o = \text{diag}[(10\ \text{km})^2, \quad (10\ \text{km})^2, \quad (10\ \text{km})^2, \quad (3\ \text{m/s})^2, \quad (3\ \text{m/s})^2, \quad (3\ \text{m/s})^2] \qquad (20)$$

The process noises for acceleration uncertainty are set to 1×10^{-6}. The step size is 20 s for a 2 d simulation. After simulation, the ARSS for the two models excluding the transient state; first 20 h are 2.304 2 km (two body with J2 effect) and 2.020 4 km (J4 with drag). The RSS position error is presented in Fig. 1. It is seen that there is a small difference between the two models at that altitude .

It has to be also noted that including J4 and drag effects means that the acceleration is no longer a function of position only but also it depends on velocity, and hence an extra burden on the numerical integration function will be added. Little accuracy gained compared to the extra computations proves the suitability of the model in subsection 1.2.

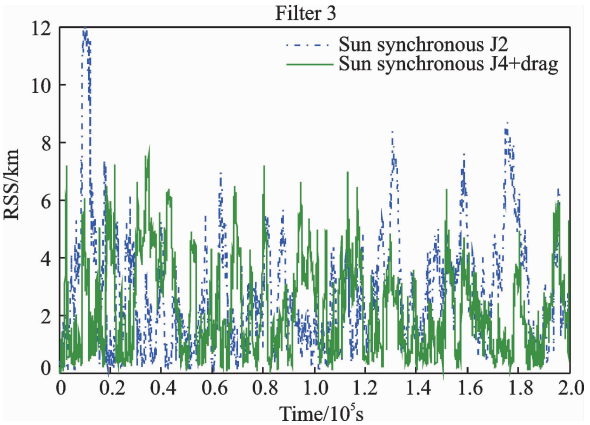

Fig. 1 Position error of the Sun synchronous orbit with different force models

In addition, including high fidelity force models in $\boldsymbol{\Phi}$ offers little advantage in accuracy and greatly increases the computational burden[23]. $\boldsymbol{\Phi}$ will also include the two bodies with J2 perturbations.

2.2 Simulation and results

The three filters are tested together with the same Sun synchronous case as the previous section discribed, as well as other circular test cases having various inclinations at the same altitude. In particular, a 5° inclined orbit representing a near equatorial orbit, 25°and 75°. The initial error is increased to be more realistic. The filter initial state vector is set an Eq. (21).

And the initial covariance is set

$$\boldsymbol{r}_o = \boldsymbol{r}_{\text{true}} + [100 \quad 100 \quad 100] \quad \text{km}$$
$$\boldsymbol{v}_o = \boldsymbol{v}_{\text{true}} + [100 \quad 100 \quad 100] \quad \text{m/s} \qquad (21)$$
$$\boldsymbol{P}_o = \text{diag}[(100\ \text{km})^2, \quad (100\ \text{km})^2, \quad (100\ \text{km})^2, \quad (100\ \text{m/s})2, \quad (100\ \text{m/s})^2, \quad (100\ \text{m/s})^2] \qquad (22)$$

The process noises for acceleration uncertainty are set as 1×10^{-6}. The RSS position error resulting from testing the three filters for the sun synchronous case is depicted in Fig. 2 and the other test cases, RSS position error for Filters 1, 2

and 3 are depicted in Figs. 3—5, respectively. ARSS values are tabulated in Table 2, they are obtained excluding the transient state first 20 h for high inclinations and 30 h for low inclination cases [9].

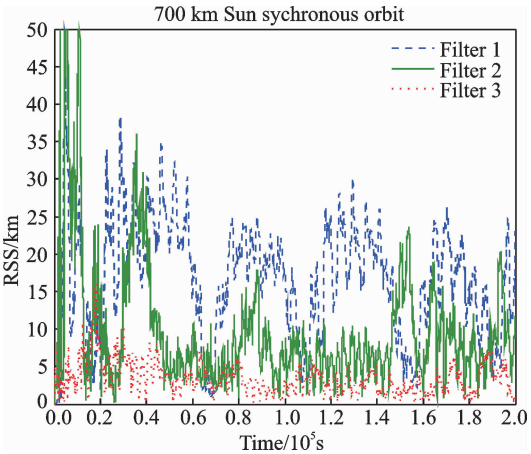

Fig. 2 Position error difference for the three filters

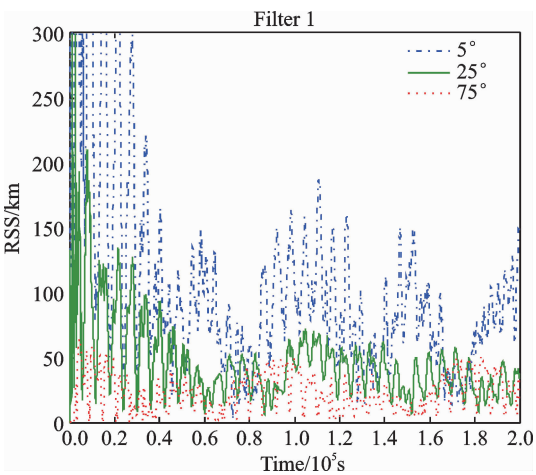

Fig. 3 Results for the position error of Filter 1 for orbits at inclinations 5°, 25°and 75°

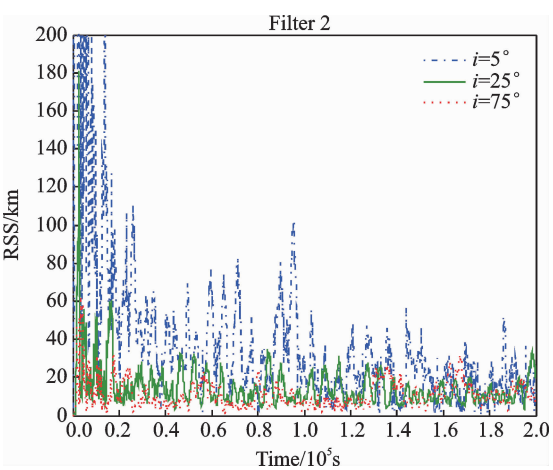

Fig. 4 Results for the position error of Filter 2 for orbits at inclinations 5°, 25°and 75°

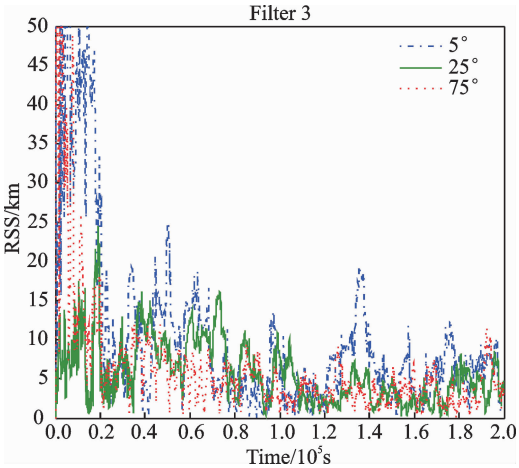

Fig. 5 Results for the position error of Filter 3 for orbits at inclinations 5°, 25°and 75°

Table 2 ARSS values results Km

Inclination	Filter 1 ARSS	Filter 2 ARSS	Filter 3 ARSS
Sun-synchronous	15.378 2	7.566 9	2.845 8
75°	20.050 0	9.388 0	3.965 4
25°	36.523 6	11.675 5	4.800 3
5°	79.824 7	25.119 0	6.453 8

The analysis and results of simulations can be summarized as follows.

The earth′s magnetic field resembles the field produced by a dipole magnet. So the field lines are more intense at the poles and become less present at lower inclinations. More field lines lead to larger partial derivatives in $\boldsymbol{H}$ matrix providing more information to correct the state.

The Sun synchronous case exhibits the best results in all filters, seen from Table 2. The first reason for the better results is that it has the highest inclination. The second is the orbits nature, being constantly oriented towards the sun during the year, which make the dual based filter more valuable. Fig. 2 compares the RSS of the three filters for the Sun synchronous case.

Particularly Filters 1 and 2 are important in the analysis as they deployed the magnetic table. Moreover, the reason for defining Filter 1 in the analysis is to see what accuracy the magnetic table provides with magnetometer data only in case of the Sun sensor suffers any malfunction on board. Results of the filters are important to be com-

pared together. Filter 1, resulted in convergence in lower inclinations but very high error. When including the Sun sensor measurements (Filter 2), the error dropped to nearly one third the error that resulting from Filter 1 at lower inclinations (seen from Table 2 when comparing the two filter results in cases 5° and 25°). As the inclination increases, the difference between Filters 1 and 2 decreased (seen when comparing the two filter results of the sun synchronous and 75°test cases). It is concluded that at low inclinations more than one measurement type is preferred for better accuracy.

As the inclination increases, the position errors decreases, which reveals that the inclination is an important parameter that affects this study (seen through Figs. 2—4).

The pure filter performance is seen by Filter 3 as it is free from modeling errors. It presents the lowest RSS position error compared with Filters 1 and 2 but it is not practical for CubeSat usage. Filter 2 presents a more realistic option than Filter 3 for on-board AOD. Its accuracy is acceptable ranging from 7.5 km to 25 km in the test cases chosen for the analysis as tabulated in Table 2.

3 Conclusions

AOD based on integrated magnetometer and sun sensor data has been explored for CubeSats. EKF has been adopted in the system to provide the states estimates.

A magnetic table was proposed to generate the reference magnetic filed with a low computational burden. The main advantage of the proposed model is that it could provide a more realistic and practical option to be used onboard CubeSats.

The accuracy provided by the table has been determined and analyzed through simulations. For this purpose three EKFs were applied with different calculation models and data types. The filter adopting the table and using both sensor measurements resulted in moderate accuracy which is sufficient for most CubeSat missions. The ARSS ranged from 7.5 km to 25 km in the examined test cases. Through the analysis it was seen that filters′ results greatly dependent on the inclination of the orbit.

For future work, the filters can also be tested with different sampling rates. Longer sampling rates are preferred for small satellites due to their limited computational power. Another aspect is also to test the filter with real data. When the filter is further tested with real data, performing simulations to try to recreate the deteriorated accuracy seen by flight data compared to simulated data, could be beneficial for understanding the filter.

Acknowledgment

The research was supported by the Research Fund for the Doctoral Program of Higher Education of China (No. 20113219110025).

References:

[1] O′KEEFE S A. Autonomous sun-direction estimation using partially under determined coarse sun sensor con? gurations [D]. Colorado: University of Colorado, 2015.

[2] PUIG-SUARI J, TURNER C, TWIGGS R J. CubeSat: The development and launch support infrastructure for eighteen different satellite customers on one launch [C] // Proceedings of the AIAA/USU Conference on Small Satellites. Logan, UT: AIAA, 2001: 1-5.

[3] BOUWMEESTER J, GUO J. Survey of worldwide pico and nanosatellite missions, distributions and subsystem technology [J]. Acta Astronautica, 2010, 67(7/8): 854-862.

[4] GILL E, SUNDARAMOORTHY P, BOUWMEESTER J, et al. Formation flying within a constellation of nano-satellites [J]. Acta Astronautica, 2013, 82(1):110-117.

[5] LONG A C, LEUNG D, FOLTA D, et al. Autonomous navigation of high-earth satellites using celestial objects and Doppler measurements [C] // Proceedings of the AIAA/AAS Astrodynamics Specialist Conference. Denver, USA: AIAA, 2000.

[6] PSIAKKI M, MARTEL F. Autonomous magnetic navigation for earth orbiting spacecraft [C] // Third Annual AIAA/USU Conference on small Satellites. [S. l.]: AIAA, 1989.

[7] MATTHIAS W. Autonomous satellite navigation via Kalman filtering of magnetometer data [J]. Acta Astronautica, 1996, 38 (4/5/6/7/8): 395-403.

[8] WU J J. Particle filter using a new resampling approach applied to LEO satellite autonomous orbit determination with a magnetometer [J]. Acta Astronautica, 2012, 81 (2): 512-522.

[9] ROH K M, PARK S Y, CHOI K H. Orbit determination using the geomagnetic field measurement via the unscented Kalman filter [J]. Journal of Spacecraft and Rockets, 2007, 44 (1): 246-253.

[10] DEUTSCHMANN J, HARMAN R, ITZHACK Y, et al. A low cost approach to simultaneous orbit, attitude, and rate estimation using an Extended Kalman Filter [C] // AAS/GSFC 13th International Symposium on Space Flight Dynamics. Maryland:[s. n.],1998.

[11] ABDELRAHMAN M, PARK S Y. Simultaneous spacecraft attitude and orbit estimation using magnetic field vector measurements [J]. Aerospace Science Technology, 2011, 15(8):653-669.

[12] SHORSHI G, ITZHACK Y, ITZHACK B. Satellite autonomous navigation based on magnetic field measurements [J]. Journal of Guidance, Control and Dynamics, 2012, 18 (4): 843-850.

[13] PSIAKI M L. Autonomous LEO orbit determination from magnetometer and sun sensor data [J]. Journal of Guidance, Control and Dynamics, 2010, 22 (2): 296-304.

[14] PSIAKI M L. Autonomous orbit and magnetic field determination using magnetometer and star sensor data [J]. Journal of Guidance, Control and Dynamics, 1995, 18 (3): 584-592.

[15] FARAHANIFAR M, ASSADIAN N. Integrated magnetometer-horizon sensor low-earth orbit determination using UKF [J]. Acta Astronautica, 2015, 106: 13-23.

[16] NING X L, MA X, PENG C, et al. Analysis of filtering methods for satellite autonomous orbit determination using celestial and geomagnetic measurement [J]. Mathematical Problems in Engineering, 2012(1024-123X): 95-100.

[17] KE H, HAO W, BINJIEET T, et al. Pico-satellite autonomous navigation with magnetometer and sun sensor data (ELSEVIER) [J]. Chinese Journal of Aeronautics, 2010, 24 (1): 46-54.

[18] OTTMARK R. Autonomous satellite orbit determination based on magnetometer and sun sensor measurements design, test and verication[D]. Swed Chin J Aeronaut en: Lulea University of Technology, 2015.

[19] EL-MAHY M K. An investigation into Kalman Filter target tracking algorithms and their real time parallel transputer implementation [D]. Cranfield: Cranfield University, 1994.

[20] HENDY H, RUI X T, KHALIL M. An integrated GPS/INS navigation system for land vehicle [J]. Applied Mechanics and Materials, 2013, 336/337/338: 221-226.

[21] GARCIA A L. Numerical methods for physics [J]. Prentice Hall, 2000, 9 (1): 55-55.

[22] ERWAN T. International geomagnetic reference field: the 12th generation [J]. Earth, Planets and Space, 2015, 67 (1): 79.

[23] VALLADO D. Fundamentals of astrodynamics and applications [M]. Space Technology Series, McGraw-Hill, USA, 2011.

Dr. **Wesam Mohammed Elmahy** received the B. S. and M. S. degrees in space science from Cairo University, the Ph. D. degree in mechanical engineering from Nanjing University of Science and Technology (NJUST), Nanjing, China, in 2007, 2011 and 2017, respectively. She was the first student of Micro-nano Satellite Research Center in NJUST and was mainly responsible for the orbit determination and control subsystem. Her research interest is autonomous orbit determination for CubeSats and microsatellites. She has participated in several satellite projects consisting of NJUST-1, NJUST-2, Bayi education CubeSat and LSSAT-1. The orbit determination algorithms studied by her was demonstrated a good performance in orbit.

Prof. **Zhang Xiang** received the Ph. D. degree in aeronautical and astronautical manufacturing from Nanjing University of Aeronautics and Astronautics (NUAA), Nanjing, China, in 2006. From 2007 to 2011, he was with the Mini-satellite Research Center in Nanjing University of Aeronautics and Astronautics, where he was the associate chief system engineer of the TX-1 mini-satellite. Since January of 2012, he has been with Nanjing University of Science and Technology (NJUST), Nanjing, China, where he is currently an Associate Professor with the School of Mechanical Engineering and the Dean of Mini/Micro Satellite Center of NJUST. He is the Project Manager of a number of satellite projects organized by European QB50 committee, or funded by Chinese General Armament Department, the Chinese Astronautical Institutes and NJUST. Currently, he takes in charge of the design and manufacture of three CubeSats, NJUST-1 (one of the 50 CubeSats in QB50 project), NJUST-2 (collaborated with Shanghai Mini-satellite Re-

search Institute) and NJFA-1 (Bio-CubeSat collaborated with Agriculture Science Academy of Fujian Province). His research interest is mini-satellite technology, including system and structural design, system assembly, system testing, etc.

Dr. **Lu Zhengliang** received the Ph. D. degree in mechanical engineering from Nanjing University of Science and Technology (NJUST), from 2012 to 2017, Nanjing, China. He was among the earliest group of Micro-nano Satellite Research Center in NJUST and was mainly responsible for the attitude determination and control subsystem (ADCS). He had conducted a deep study on the attitude determination algorithm and attitude control law for micro satellites. He has participated in several satellite projects as a major member. These projects consist of NJUST-1 (collaborated with Shanghai Microsatellite Research Institute), NJUST-2 (one of the 50 CubeSats in QB50 project, organized by European QB50 committee), Bayi education CubeSat (science education for senior high school student) and LSSAT-1 (high resolution optical satellite). His research interest is advanced ADCS technology with high-precision pointing control and high stability.

Prof. **Liao Wenhe** received the B. S. degree in aircraft manufacturing engineering, the M. S. and Ph. D. degrees in aeronautical and astronautical manufacturing from Nanjing University of Aeronautics and Astronautics (NUAA), Nanjing, China, in 1985, 1990 and 1996, respectively. In 1996, he was appointed as a professor for mechanical engineering in NUAA. In 2010, he was appointed as the vice president of Nanjing University of Science and Technology. Since 1996, he initiated and supervised research activities in various aspects of the digital design and manufacturing technologies for aeronautical and astronautical products in NUAA. Numerous achievements with independent intellectual property rights have been obtained and widely applied in practical product manufacturing. From 2005 to 2010, he was the principle investigator for the NUAA TX-1 mini-satellite project, where TX-1 is one of the very few micro-satellites developed independently by the Chinese universities. He was also the chief system engineer of TX-1, taking charge of the design of the satellite system, system assembly, integration and testing, quality control and the management of the team. His current research interests are mini/micro-satellite techniques, airplane three-dimensional (3D) digital design, digital assembly and high-precision digital medical equipment. He is the author of two textbooks and has published more than 120 papers in various international journals and conferences.

(Executive Editor: Zhang Bei)